Available online at www.sciencedirect.com

SciVerse ScienceDirect

Ceramics International 39 (2013) 983–990

CERAMICS INTERNATIONAL

www.elsevier.com/locate/ceramint

Preparation and properties of sol–gel synthesized Mg-substituted Ni_2Y hexagonal ferrites

Asmat Elahi, Mukhtar Ahmad, Ihsan Ali, M.U. Rana*

Department of Physics, Bahauddin Zakariya University, Multan 60800, Pakistan

Received 26 February 2012; received in revised form 16 June 2012; accepted 4 July 2012
Available online 23 July 2012

Abstract

A series of single phased Y-type hexagonal ferrites $Sr_2Ni_{2-x}Mg_xFe_{12}O_{22}$ ($x=0.0$, 0.1, 0.2, 0.3, 0.4, 0.5) were synthesized by the sol–gel auto combustion method. The effects on structural, magnetic and electrical properties have been investigated by substituting Mg^{2+} at Ni^{2+} sites. The X-ray diffraction (XRD) patterns confirm single phase Y-type hexaferrite and various parameters such as lattice constants, cell volume, X-ray density, bulk density and porosity have been calculated from XRD data. The Fourier transform infrared (FTIR) spectra show the characteristics absorption ferrite peaks of the sintered sample. The microstructure was studied by scanning electron microscopy (SEM). All the ferrites show a hexagonal platelet-like shape which is a most suitable shape for microwave absorption. The dielectric constant followed the Maxwell–Wagner interfacial polarization and relaxation peaks were observed in the dielectric loss properties. The room temperature dc electrical resistivity and activation energy were found to decrease for samples $x=0.1$, 0.2 and increase for the rest of samples hence making these materials suitable for multilayer chip inductors (MLCIs). A soft magnetic behavior was revealed by M–H loops. Saturation magnetization (M_s), retentivity (M_r), coercivity (H_c) and magnetic moment (n_B) were found to decrease as the Mg^{2+} contents increased.

Keywords: Y-type hexaferrites; Microstructure; Dielectric measurements; M–H loops

1. Introduction

Hexagonal ferrites have a wide range of applications in the field of materials science. The family of hexagonal ferrites can be classified on the basis of chemical composition and crystal structure. These are subdivided into five fundamental and simplest structural types: M, W, Y, X and Z [1]. Gorter [2] made the first attempt to determine the position of the magnetic ions and orientation of the spins in the crystal lattice by considering exchange interactions. It was observed that the spins are collinear in the basal plane particularly in Y-type hexagonal structure. The structure of Y-type hexaferrite has space group (R3m) and is often designated as $(TS)''|(TS)(TS)'\ (TS)''|(TS)$—, where the prime means the block is rotated 120° around the c-axis [3]. The structure consists of three Y blocks (formula units). Each Y block consists of two layered spinel S block and four-layered antiferromagnetic T block. The metallic cations in the blocks occupy either tetrahedral or octahedral sites between the oxygen polyhedra [4]. The knowledge of the distribution of cations is of utmost importance in understanding their physical and chemical properties. Due to their magneto-dielectric properties, hexaferrites play an important role in the field of electronic industry. The magnetic properties of hexaferrites have been studied extensively [5–8]. Y-type hexaferrites provide a useful combination of ferrimagnetic and insulating properties and are well known for their use as magneto-electric devices. Also these materials have high initial magnetic permeability and high resistivity and for this reason these are considered as suitable in hyper frequency regions (300–1000 MHz) as well as multilayer chip inductors (MLCIs) and multilayer chip beads (MLCBs). Moreover, Y-type hexagonal ferrites exhibit excellent magnetic properties also in hyper-frequency region, and are good candidates as soft-magnetic materials for chip components [9]. Besides

*Corresponding author. Tel.: +92 61 9210199; fax: +92 61 9210068.
E-mail addresses: mazharrana@bzu.edu.pk, ahmadmr25@yahoo.com (M.U. Rana).

0272-8842/$ - see front matter © 2012 Elsevier Ltd and Techna Group S.r.l. All rights reserved.
http://dx.doi.org/10.1016/j.ceramint.2012.07.016

magnetic properties, the dielectric constant of ferrite materials is also crucial for MLCIs [10]. In the multi-layer structure, the unavoidable wiring capacity is resonated with inductance and limits the cut-off frequency of inductive components. Therefore, low permittivity is expected to optimize the frequency character of inductive components. The sol–gel technique is receiving much attention because it can be applied to prepare an extremely wide variety of materials. This technique also offers the possibility of controlling not only the size and distribution of particles but also their shape.

In the present work, strontium based Y-type hexaferrites were substituted with Mg^{2+} ions at Ni^{2+} sites in order to study the structural, electrical and magnetic properties of these ferrites. The objective of this research work is, by using sol–gel technique, to prepare a core material with high resistivity and lower coercivity which must have applications in hyper frequency regions.

2. Experimental

A series of single phase Y-type hexagonal ferrites of composition $Sr_2Ni_{2-x}Mg_xFe_{12}O_{22}$ (x=0.0, 0.1, 0.2, 0.3, 0.4, 0.5) were synthesized by the sol–gel auto combustion method. $Sr(NO_3)_2$ (>99%, Sigma Aldrich, Germany), NiO (>99%, Merck, Germany), $Fe(NO_3)_3\cdot 9H_2O$ (+98%, Sigma Aldrich, USA) and $Mg(NO_3)_2\cdot 6H_2O$ (+98%, Sigma Aldrich, UK) were used as starting materials. According to stoichiometric calculations, required amount of salts were used to make solution in 100 ml deionized water. As NiO is not soluble in deionized water, it was dissolved in nitric acid (HNO_3), heated up to 80 °C to convert it into nickel nitrate, which is a soluble salt in water. Citric acid (99.91%, Fisher Scientific, UK) was used as a chelating agent. Maintaining the pH value at about 7–8 by using ammonia solution (35%, Fisher Scientific, UK), stirring continued under temperature at 80 °C, at this temperature evaporation of deionized water started and after complete evaporation, reaction started. The reaction continued and the color of solution was golden yellow during heating process. At the end, the golden gel was formed. When temperature was increased to about 200 °C, this gel started turning into ash i.e. auto combustion was done. Heating continued till the whole gel turned into loose and fluffy powdered sample. Each sample was ground using agate mortar and pestle for 10 min to obtain a fine powder. The powder was then sintered at 1150 °C for 7 h to obtain the Y-type hexagonal ferrites. The samples were furnace cooled to obtain the equilibrium position of the cations. The powder was then pressed into pellets at a pressure of (~35 kN) for about 3 min using Paul-Otto Weber hydraulic press. Polyvinyl alcohol was used as a binder for pelletization. The pellets were kept in a furnace at 300 °C for 1 h to evaporate the binder. The X-ray diffraction (XRD) patterns were recorded at room temperature in the 2θ range 20° to 70° by using a computer controlled JDX-60PX, JEOL Boston model which was operated at 40 kV and at 30 mA. The radiation used was Cu-K_α (λ=1.5406 Å) with Ni filter. The samples for infrared (IR) studies were prepared according to the technique used by Mazen [11] by mixing the powdered sample with KBr in the ratio 1:100 by weighing to insure uniform dispersion. The IR spectra were recorded on Shimadzu 8400S IR spectrometer in the near infrared region 400–4000 cm^{-1}. The scanning electron microscope (Model: Hitachi S4160) was used to examine the morphology and to evaluate the grain size of the investigated ferrites. The DC electrical resistivity (ρ) for all these samples was measured by two-probe method, because of the high resistivity of these ferrites. In order to measure it the following relationship was employed;

$$\rho = \frac{RA}{t} \quad (1)$$

where, R, A and t, are the resistance, area of cross-section and thickness of pellet respectively.

Moreover the capacitance of all the samples was measured by LCR meter and then dielectric constant was calculated by the formula;

$$\varepsilon = Cd/A\varepsilon_o \quad (2)$$

Here C is the capacitance of a capacitor in Farad, d is the distance between the plates in a parallel plate capacitor, ε_o is the permittivity of free space (8.85×10^{-12} Fm^{-1}), and A is the cross sectional area of the flat surface of the pellet. Vibrating sample magnetometer (BHV-50, Riken Denish Company Ltd, Japan) was used in order to measure the magnetic parameters such as saturation magnetization (M_s), retentivity (M_r) and coercivity (H_c) for selected samples.

3. Results and discussion

3.1. FTIR analysis

Chemical and structural changes and the phases present in the material during combustion and sintered processes can be observed by FTIR spectroscopy. Fig. 1(a) shows the FTIR spectrum of the un-sintered powder indicating the characteristic bands of the O–H stretching vibration of water and citric acid in the 3700–2700 cm^{-1} range, while the anti-symmetrical and symmetrical stretching vibration bands of CO_2 related to citric acid are located at about 1586 cm^{-1}. The bands of NO_3 located at 1385 cm^{-1} are ascribed to the N=O, N–O stretching and bending vibration. After sintering (Fig. 1(b)), the absorption band of O–H–, CO_2– and NO_3– bands disappeared. The absorption bands at approximately 590 cm^{-1} and 433 cm^{-1} are due to the Fe–O metal–oxygen bonds, the powder sintered at 1150°C only revealed the well resolved absorption band corresponding to the metal–oxygen stretching vibration of the $Sr_2Ni_{2-x}Mg_xFe_{12}O_{22}$ single phase. The vibration bands present in the spectra at 590 cm^{-1} and 433 cm^{-1} are the common features of all the ferrites [12–15]. So it is very clear to attribute these bands to the vibrations present due to cations in the spinel block of Y ferrite. Here it may be noticed that the difference of opinion is observed from the reported data. Waldron [16] in 1955 and Hanfer and

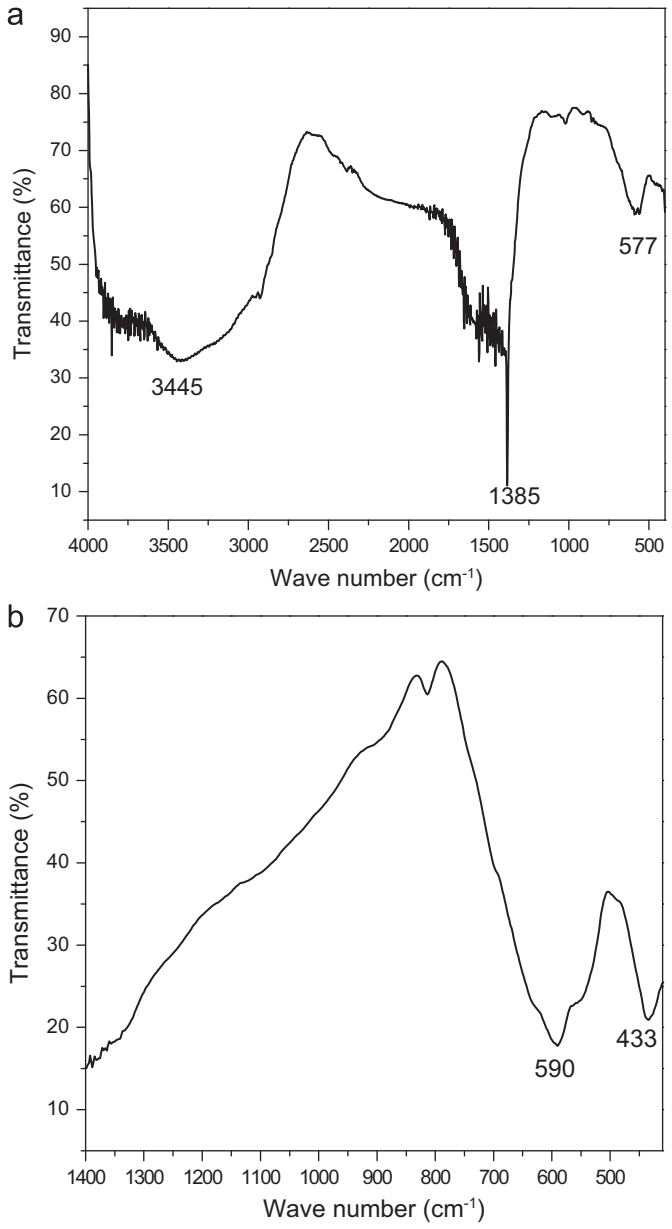

Fig. 1. FTIR spectra of an unsintered (a) and sintered (b) sample of strontium hexaferrite.

Kristaloger [17] in 1961 attributed the former band to the intrinsic vibration of tetrahedral complexes corresponding to the highest restoring force whereas the latter one is for the stretching vibrations of the octahedral group. However Preudhomme and Trate [15,18,19] verified that the above attributions are true only if the tetrahedral cations–oxygen bond is stronger or at least of the same order of magnitude than the octahedral cations–oxygen bond. For this the tetrahedral cations C_T must be of higher valence than the octahedral cation Co otherwise former band must be assigned to stretching vibration of the octahedral group. So here the absorption band at 590 cm^{-1} is assigned to the stretching vibrations of the octahedral group in the spinel blocks and the band at 433 cm^{-1} is attributed to the stretching vibrations of the tetrahedral group present in S blocks.

3.2. XRD analysis

X-ray diffraction studies were carried out to determine the structure of Y-type hexaferrites $Sr_2Ni_{2-x}Mg_xFe_{12}O_{22}$ ($x=0.0$, 0.1, 0.2, 0.3, 0.4, 0.5) samples. XRD patterns of all the samples are shown in Fig. 2 and all the peaks in XRD patterns were compared with JCPDS data (PDF # 73-2035). It reveals that the investigated ferrites were of single phase Y-type hexagonal structure. All the peaks were indexed and lattice constants (a and c) and volume of unit cell for each concentration were calculated by the following relations respectively [20,21],

$$\sin^2\theta = \frac{\lambda^2}{3a^2}(h^2+hk+k^2)+\left(\frac{\lambda^2}{4c^2}\right)l^2 \quad (3)$$

Here λ is the wavelength, a and c are the lattice constants and hkl are the corresponding Miller indices.

$$V = a^2 c \sin 120^\circ \quad (4)$$

The calculated values of lattice constants and unit cell volume are given in Table 1. It can be observed that the values are in good agreement with earlier reported values for this structure [22]. The results also show that lattice constant a of un-substituted sample is less than that of substituted samples. It is due to the difference in ionic radii of the substituted ions ($Ni^{2+}=0.69$ Å, $Mg^{2+}=0.66$ Å) [23] while c decreases because ionic radius of Mg^{2+} is less than that of Ni^{2+}. Also there is a decrease in the intensity of (113) peak in XRD patterns with addition of Mg^{2+} ions concentration. This decrease infers that the Ni^{2+} preferentially occupied the octahedral B-site on the (113) plane [23].

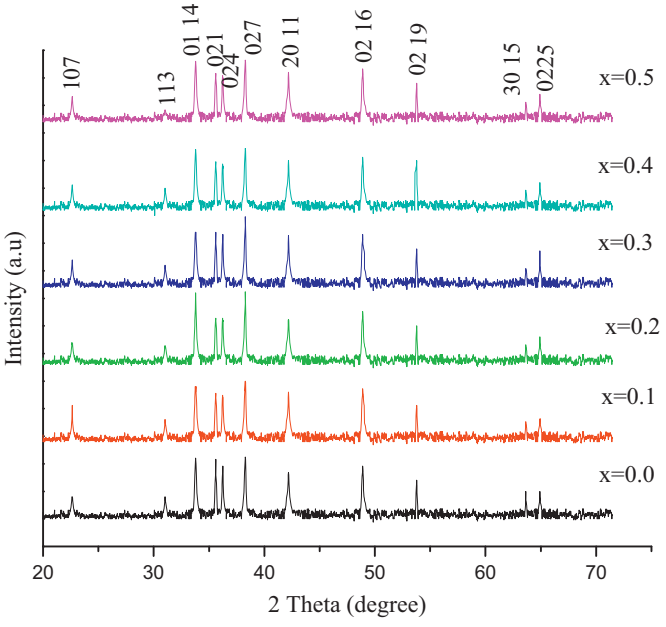

Fig. 2. XRD patterns of strontium hexaferrite $Sr_2Ni_{2-x}Mg_xFe_{12}O_{22}$ with different compositions ($x=0.0$–0.5).

Table 1
Values of different parameters calculated for Mg-substituted Ni_2Y-hexagonal ferrites.

Parameters	$x=0.0$	$x=0.1$	$x=0.2$	$x=0.3$	$x=0.4$	$x=0.5$
Lattice constant a (Å)	5.88	5.90	5.90	5.91	5.91	5.80
Lattice constant c (Å)	43.45	43.40	43.35	43.15	43.15	43.40
Cell volume (Å^3)	1301	1308.3	1308.3	1305.1	1305.1	1264.33
X-ray density (g/cm^3)	5.200	5.020	5.010	5.010	4.980	4.965
Bulk density (g/cm^3) $\pm$ 0.01	4.71	4.70	4.64	4.52	3.97	3.48
Porosity (fraction)	0.09	0.06	0.07	0.09	0.20	0.29
Resistivity (Ω-cm)	6.09×10^6	6.38×10^5	4.21×10^5	3.2×10^6	5.79×10^6	7.52×10^6
Activation energy (eV)	0.3474	0.2937	0.2883	0.4620	0.4860	0.5032

3.3. Physical properties

Bulk density plays a key role in analyzing the ferrite materials and in the present study it was calculated by the relation [24];

$$d_B = \frac{m}{\pi r^2 h} \quad (5)$$

where m, r and h are the mass, radius and thickness of the pellets respectively. The values of bulk density for all the samples are listed in Table 1. It is evident that bulk density shows a decreasing trend by increasing the Mg^{2+} concentration in Y-type hexaferrites. The decreasing behavior of the bulk density is attributed to the fact that atomic weight and density of Mg (24.30 amu, 1.74 g/cm^3) are less than that of Ni (58.69 amu, 8.91 g/cm^3) [25]. X-ray density of all the samples was also calculated by the formula [26];

$$d_x = \frac{3M}{N_A V} \quad (6)$$

where Z is 3 because the hexagonal unit cell in Y-type ferrite is composed of three overlapping T and S blocks (3(TS)) and of 18 oxygen layers [22], M is molar mass, N_A is Avogadro number and V is the unit cell volume. The values of X-ray densities are listed in Table 1. It is clear that X-ray density decreases by the increase of Mg^{2+} concentration in Y-type hexagonal ferrites. The decrease in X-ray density can be explained by the fact that density of Mg atom (1.74 g/cm^3) is less as compared to Ni atom (8.91 g/cm^3), also the atomic concentration of Mg is less (4.2×10^{22} cm^{-3}) than atomic concentration of Ni (9.14×10^{22} cm^{-3}) [27]. It can also be observed that the values of bulk density (d_B) were found to be in general less than those of X-ray density (d_x), which was expected due to the presence of unavoidable pores created during sintering process [28]. Moreover the porosity (P) of all the samples was calculated by the relation [29];

$$P = 1 - \frac{d_B}{d_x} \quad (7)$$

The values of porosity for all the samples are listed in the Table 1. It is clear that value of porosity increases by increasing Mg concentration for all samples. This increase in porosity can be attributed to the decrease in bulk density [27].

3.4. Morphology

Fig. 3 reflects the representative SEM micrographs of the investigated ferrites. All the samples show a well defined hexagonal platelet-like shape, which is a most suitable shape for microwave absorbing purposes [28]. Moreover, the grain was smaller, more perfect and homogeneous for the ferrites substituted with Mg^{2+} (average grain size 0.74–1.01 μm) than that of pure ferrite (average grain size 1.11 μm). It might be attributed to the Mg^{2+} ions having smaller value of ionic radius which were substituted in the ferrite.

3.5. Room temperature resistivity

The measured values of room temperature resistivity for all the samples have been listed in the Table 1. It is observed that resistivity decreases firstly up to $x=0.2$ and then increases for rest of the samples hence making these materials suitable for multilayer chip inductors (MLCIs). The decrease in resistivity by addition of Mg^{2+} ions indicating the preferential occupation of Mg^{2+} ions at A-sites resulting a migration of Fe^{3+} ions into the octahedral sites. The increase in concentration of Fe^{3+} ions at B-sites increases the hoping rate of electrons, which in turn enhances the conductivity to maximum. In the second case it increases due to the fact that the Mg^{2+} ions go to B-sites. Now the ferrous and ferric ions are not available at B-sites and hence there is low specific conductivity or high resistivity [29].

3.6. Temperature dependent resistivity

Temperature dependent resistivity of these samples was measured in the temperature range of 303–453 K. Fig. 4 exhibits the behavior of electrical resistivity as a function of temperature. A sharp decrease in resistivity with increase in temperature is observed due to hopping of electrons. Moreover at low temperature the deleterious effect of some impurities may increase resistivity, but at higher temperature this influence becomes negligible. The conduction mechanism can be explained by Verwey et al. [30] hopping mechanism. According to Verwey, the conduction mechanism in ferrites occurs mainly through the

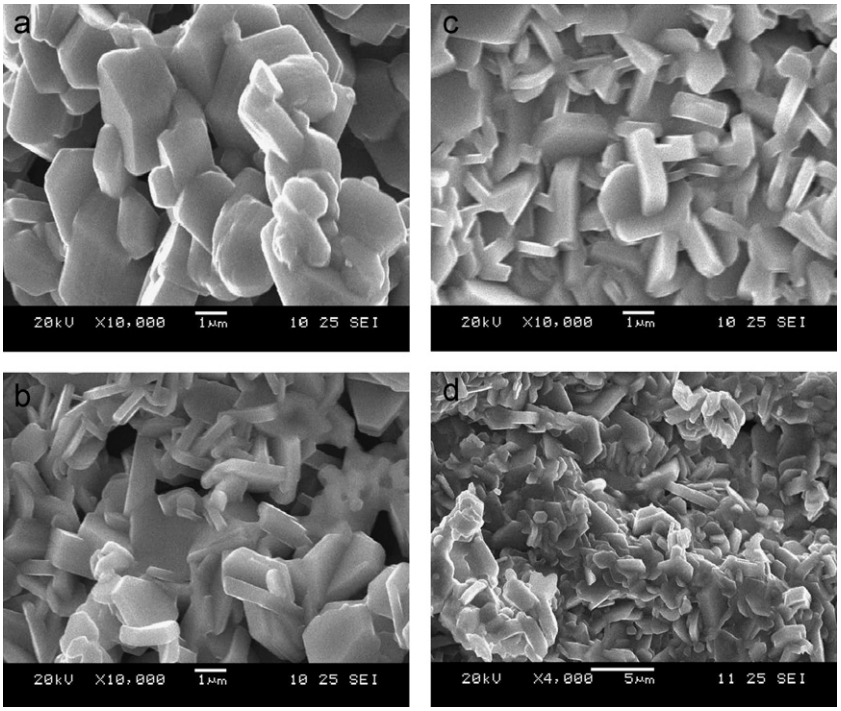

Fig. 3. SEM images (a–d) of strontium hexaferrite $Sr_2Ni_{2-x}Mg_xFe_{12}O_{22}$ for $x=0.0$, 0.2, 0.4, and 0.5.

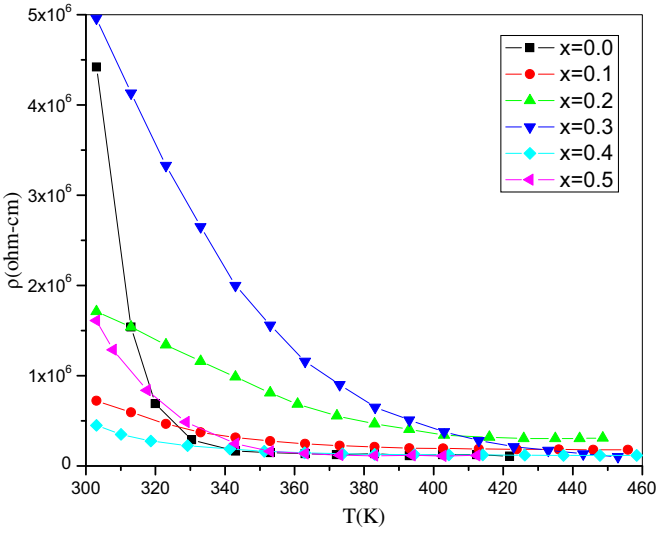

Fig. 4. Variation of resistivity (ρ) with temperature for $Sr_2Ni_{2-x}Mg_xFe_{12}O_{22}$ ($x=0.0$–0.5) hexaferrites.

hopping of electrons between Fe^{2+} and Fe^{3+}, the ions of the same elements distributed randomly on B-sites. The number of such ions depends upon the sintering conditions and the reduction of Fe^{3+} and Fe^{2+} ions at elevated temperature [31]. Also hole hopping between Ni^{2+} and Ni^{3+} ions on B-sites will contribute to electric conduction in ferrites. In the present work, the hole conduction depends on Mg^{2+} concentration at the expense of Ni^{2+} concentration. The activation energy was calculated from the plots of $\ln \rho$ versus $1000/T$ for all the samples. Activation energy showed the Arrhenius type temperature dependence in the range of 303–453 K i.e.

$$\rho = \rho_o e^{E_a/kT} \quad (8)$$

where ρ_o is resistivity at room temperature, k is Boltzmann constant (1.38×10^{-23} J K^{-1}), E_a is activation energy and T is absolute temperature. The value of activation energy was calculated from the slope of the resistivity versus temperature graph. The value of activation energy E_a was found to decrease for samples $x=0.0$, 0.1, 0.2 and then there was an increase for rest of the samples, with increases in Mg^{2+} content (Table 1). It was expected because the sample with low resistivity value has low value of activation energy and vice versa [23].

3.7. Dielectric properties

The dielectric behavior is one of the most important characteristics of ferrites which markedly depend on the preparation conditions, e.g. sintering time and temperature, type and quantity of additives. The frequency dependence of the dielectric constant for all samples is shown in Fig. 5. It is seen that dielectric constant decreases with increasing frequency and then reaches a constant value. The observed variation can be explained on the basis of space charge polarization. According to the two-layer model of Maxwell and Wagner, which is in agreement with Koop's phenomenological theory [32–34] the space charge polarization arises due to inhomogeneous dielectric structure of the material. It is composed of large well conducting grains separated by thin poorly or non-conducting inter-grain boundaries. The bi-layer formation results by high temperature sintering. The polarization

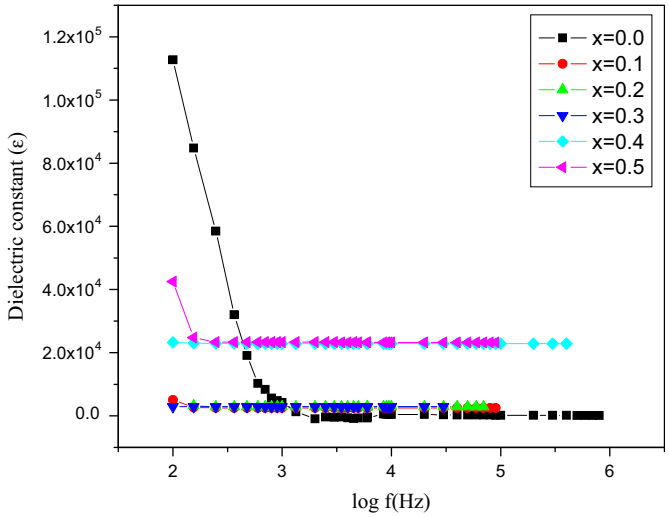

Fig. 5. Frequency dependence of the dielectric constant (ε) of strontium hexaferrite $Sr_2Ni_{2-x}Mg_xFe_{12}O_{22}$ (x=0.0–0.5).

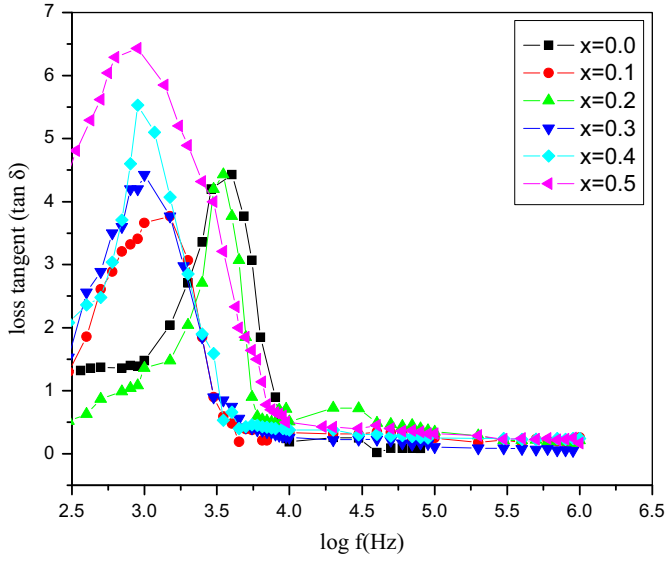

Fig.6. Frequency dependence of the tangent loss (tan δ) of Mg-substituted Ni_2Y-hexagonal ferrites (x=0.0–0.5).

takes place in an electronic exchange between the ferrous and ferric ions, which produce local displacements in the direction of applied external fields. Similarly the $Ni^{3+} \leftrightarrow Ni^{2+} + e^{+}$ gives the hole concentration in the octahedral sites which produce the local displacements in the opposite direction of the applied fields. The observed behavior of dielectric constant decreases with increase in frequency is due to the fact that above certain frequencies the electronic exchange between the ferrous and ferric ions does not follow the applied field. The large value of dielectric constant at lower frequency may also be due to the predominance of species like Fe^{2+} ions, interfacial dislocations, piles up, oxygen vacancies, grain boundary, defects etc [33,34]. Whereas the decrease in dielectric constant with frequency is natural due to the fact that any species contributing to polarizability is found to show lagging behind the applied field at some higher frequencies. Among all the samples, the lower dielectric constant value is observed for the $Sr_2Ni_{1.5}Mg_{0.5}Fe_{12}O_{22}$ sample, because of the unavailability of ferrous and ferric ions in the octahedral sites, which are preferentially occupied by Mg^{2+} ions. Moreover the dielectric constant of all the samples was calculated by the Eq. (2) [35,36]. Fig. 6 shows the variation of loss tangent with frequency for the samples of $Sr_2Ni_{2-x}Mg_xFe_{12}O_{22}$ hexaferrites. It can be seen that an abnormal dielectric behavior was observed for all the samples because of the fact that dielectric relaxation peaks were found. According to Rezlescu model the relaxation peaks may be due to the collective contribution of both p and n type of charge carriers [37]. The electronic exchange between Fe^{3+} and Fe^{2+} and hole transfer between Ni^{2+} and Ni^{3+} in the octahedral sites are responsible for such behaviors. Furthermore the jumping frequencies of localized charge carriers are almost equal to that of the applied electric field [23].

3.8. Magnetic properties

The M–H loops measured at room temperature for some selected samples (x=0.0, 0.3, 0.5) are shown in Fig. 7. The magnetic parameters such as saturation magnetization (M_s), coercivity (H_c), retentivity (M_r), squareness and magnetic moment (n_B) were obtained from the loops and are listed in Table 2. It is evident that values of all these parameters lie in the range of earlier reported values for this structure [38]. It is also clear that saturation magnetization (M_s), retentivity (M_r), coercivity (H_c) and magnetic moment (n_B) decrease with the increase of Mg contents. The variation of these parameters as a function of Mg concentration is shown in Fig. 8. The decrease in M_s and M_r can be explained on the basis of magnetic character and anisotropic nature of Mg^{2+} ions. This decrease suggested

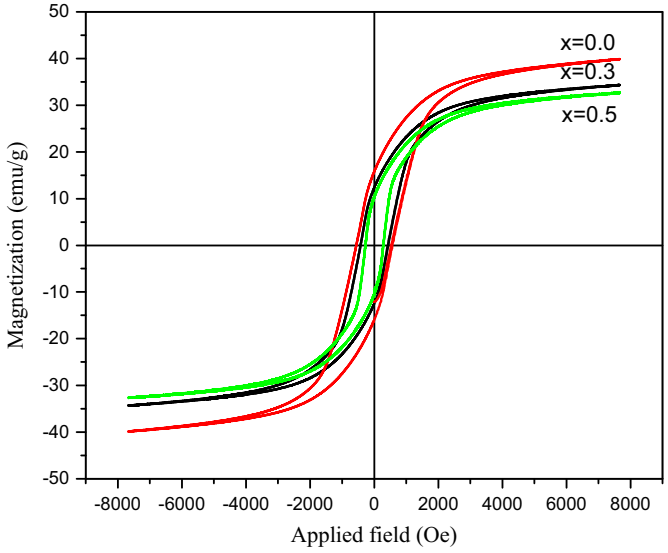

Fig. 7. Hysteresis loops for Mg-substituted Ni_2Y-hexagonal ferrites for x=0.0, 0.3, and 0.5.

Table 2
Values of saturation magnetization (M_s), retentivity (M_r), squareness, magnetic moment (n_B) and coercivity (H_c) for $x=0.0$, 0.3, 0.5.

Samples x	M_s (emu/g)	M_r (emu/g)	Squareness M_r/M_s	n_B (μ_B)	H_c (Oe)
0.0	40.34	16.68	0.410	9.94	555.44
0.3	34.44	13.44	0.390	8.04	437.21
0.5	32.84	10.65	0.324	7.63	276.06

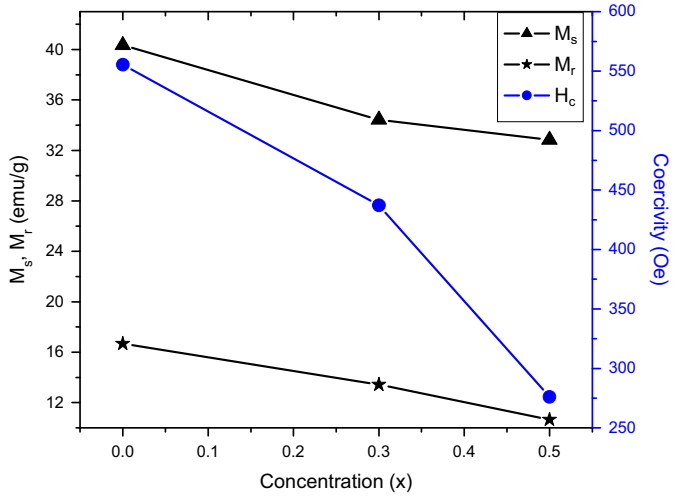

Fig. 8. Variation of saturation magnetization (M_s), retentivity (M_r) and coercivity (H_c) with concentration (x).

the decrease of strongly interacted magnetic state towards a less magnetized state [39]. The magnetic order of S-block was due to super exchange interaction mechanism of metal ions between A and B sites. The replacement of Ni^{2+} ions by Mg^{2+} ions (having zero magnetic moment) which had B-site occupancy resulted in the reduction of super exchange interaction between A and B sites. In other meaning as Mg^{2+} concentration increased, the magnetization of B-sites M_B decreased while that of A site M_A remained constant. As net magnetization is equal to M_B-M_A so it was found to decrease. Moreover the decrease in H_c with Mg^{2+} contents was due to the reason that the anisotropy constant value of Ni ferrite is greater than that of Mg ferrite. So the replacement of Ni^{2+} by Mg^{2+} ions leads to a decrease in coercivity values for the investigated Y-type hexagonal ferrites [38].

4. Conclusion

Single phased Y-type hexagonal ferrites $Sr_2Ni_{2-x}Mg_xFe_{12}O_{22}$ have been synthesized successfully by using sol–gel followed by an auto combustion method. The XRD data reveal that all the synthesized samples are single phase. The FTIR spectra show the characteristics peaks of the ferrite system. The SEM images reveal that the grain is smaller and more homogeneous for Mg^{2+} substituted ferrite than the pure ferrite. All the ferrites show a hexagonal platelet-like shape which is a better shape for microwave absorption. The room temperature dc electrical resistivity was found to decrease for $x=0.0$–0.2 and increases for rest of the samples. The dielectric constant decreased with increase of frequency due to electronic exchange between Fe^{2+} and Fe^{3+} satisfying the Koop's phenomenological theory. The variation of loss tangent with frequency showed an abnormal dielectric behavior for all the samples. Relaxation peaks resulted and it might be due to the collective contribution of both p- and n-type of charge carriers. Saturation magnetization (M_s), retentivity (M_r), coercivity (H_c) and magnetic moment (n_B) were found to decrease with the increase of Mg content. Owing to all these distinguished parameters, it can be affirmed that these materials are suitable for multilayer chip inductors (MLCIs) and multilayer chip beads (MLCBs) as high resistivity and low coercivity are basic requirements for these applications.

Acknowledgment

Dr. M.S. Awan (COMSATS) Islamabad and M. Aleem (UGS, BZU) Multan are highly acknowledged to provide SEM images and IR spectra, respectively.

References

[1] J. Smit, H.P.J. Wijn, Ferrites, Philip's Technical Library, New York, 1959.
[2] E.W. Gorter, Magnetism, materials and applications, Proceedings of IEE (London) 104B (Suppl 5) (1957) 255.
[3] G. Albanese, M. Carbucicchio, A. Deriu, G. Asti, S. Rinaldi, Cation distribution and helimagnetic structure of $Ba_2(Zn_{1-x}Mg_x)_2Fe_{12}O_{22}$, Applied Physics 7 (1975) 227.
[4] L.R. Bickford, Anisotropy and Magnetostriction in Magnetic Oxides, Physical Review 119 (1960) 1000.
[5] X.Z. Zhou, A.H. Morrish, Studies of static and high frequency magnetic properties of M-type ferrite $BaFe_{12-2x}Co_xZr_xO_{19}$, Journal of Applied Physics 75 (10) (1994) 5556.
[6] H.J. Kwon, Journal of Applied Physics 75 (10) (1994) 6109.
[7] F.K. Lorgering, P.R. Locher, R.P. Van Stanperf, Dielectric dispersion of Y-type hexaferrites at low frequencies, Journal of Physics and Chemistry of Solids 41 (1980) 481.
[8] E. Naiden, G. Ryabsten, Thermoelectric power and electrical conductivity of Cu–Ti ferrite, Sov. Phys. J. 33 (1990) 318.
[9] S.A. Saafan, A.M. Abo El Ata, M.S. El Messeery, Journal of Magnetism and Magnetic Materials 302 (2006) 362–367.
[10] M. El-Saadawy, Journal of Magnetism and Magnetic Materials 219 (2000) 69–72.
[11] S.A. Mazen, M.H. Abdallah, B.A. Sabrals, H.A.M. Hashem, Dielectric behavior of $Cu_{1-x}Ti_x$ Fe_2O_4 ferrites, Physica Status Solidi 134 (1992) 263.
[12] P.N. Vasambekar, C.B. Kolekar, A.S. Vaigankar, Electrical switching in $Cd_xCo_{1-x}Fe_{2-y}Cr_yO_4$ system, Materials Research Bulletin 34 (6) (1999) 863.
[13] R.S. Patil, S.V. Kakatkar, A.M. Sankpal, S.R. Sawant, S.S. Suryavanshi, U.R. Ghodke, K. Kamat, Magnetic properties of mixed Li–Ni–Cd ferrites, Indian Journal of Pure and Applied Physics 32 (1994) 193.
[14] N.W. Grimes, A.J. Collet, Influence of magnetic ordering on the electrical properties of nickel ferrite-chromite ($NiFeCrO_4$) in the region of temperature compensation, Physica Status Solidi (b) 43 (1971) 591.

[15] J. Preudhomme, P. Tarte, Study of infrared spectroscopy and elastic properties of fine and coarse grained nickel–cadmium ferrites, Spectrochimica Acta 27a (1971) 1817.
[16] R.D. Waldron, Infrared spectra of ferrites, Physical Review 99 (1955) 1727.
[17] S. Hanfer, Z. Kristaloger, Electrical and magnetic properties of spinel $ZnCr_{2-x}Fe_xO_4$, 115 (1961) 331.
[18] J. Preudhomme, P. Tarte, The iron oxides: structure, properties, reactions, occurences and uses, Spectrochimica Acta 27a (1971) 961.
[19] P. Tarte, J. Preudhomme, Infrared studies of spinels-III: the normal II–III spinels, Acta Crystallographica 16 (1963) 227.
[20] B.D. Cullity, Elements of X-rays diffraction, Second ed., Addison Wesley Publishing Co., Philippines, 1978, p. 338 (Chapter 10).
[21] M.J. Iqbal, F. Liaquat, Physical and electrical properties of nano-sized Mn-and Cr-Doped Strontium Y-Type hexagonal ferrites, Journal of American Ceramic Society 93 (2010) 474.
[22] Y. Salunkhe, D. Kulkarni, Structural, magnetic and microstructural studyof $Sr_2Ni_2Fe_{12}O_{22}$, Journal of Magnetism and Magnetic Materials 279 (1) (2004) 64–68.
[23] L. John Berchmans, R. Kalai Selvan, P.N. Selva Kumar, C.O. Augustin, Strucructural and electrical properties of $Ni_{1-x}Mg_xFe_2O_4$ synthesised by citrate gel process, Journal of Magnetism and Magnetic Materials 279 (2004) 103–110.
[24] M.J. Iqbal, R.A. Khan, Enhancement of electrical and dielectric properties of Cr doped $BaZn_2W$-type hexaferrite for potential application in high frequency devices, Journal of Alloys and Compounds 374 (2009) 286–289.
[25] M. Naeem, N.A. Shah, I.H. Gull, A. Maqsood, Structural and microwave absorption properties of $Ni_{1-x}Co_xFe_2O_4$ ($0.0 \le x \le 0.5$) nanoferrites synthesized via co-precipitation route, Journal of Alloys and Compounds 487 (2009) 739–743.
[26] U. Ghazanfer, S. Siddiqi, G. Abbas, Analysis of power losses in Mn–Zn ferrites, Journal of Materials Science Engineering B 118 (1–3) (2005) 132–134.
[27] C. Kittle, Introduction to Solid State Physics, 7th ed., Wiley, New York, 1999, p.24.
[28] M.A. Ahmed, N. Okasha, M. Oaf, R.M. Kershi, Dramatic effect of rare earth ion on the electrical and magnetic properties of W-type barium hexaferrites, Journal of Magnetism and Magnetic Materials 314 (2007) 128–134.
[29] S.M. Attia, A.M. Abo El Ata, D. El Kony, Extraordinary role of rare-earth elements on the transport properties of barium W-type hexaferrite, Journal of Magnetism and Magnetic Materials 270 (2004) 142–151.
[30] E.J.W. Verwey, F. De. Boer, H.H. Vansten, Cation arrangement in spinels, Journal of Chemical Physics 161 (1948) 1901.
[31] S.N. Kulkarni, Structural and Electrical Properties of Cd-substituted Li–Ni Ferrites, Ph.D. Thesis, Shivaji University, Kolhapur, 1994.
[32] J.C. Maxwell, A Treatise on Electricity and Magnetism, vol 2, Oxford, New York, 1954.
[33] K.W. Wagner, Dielectric relaxation in distributed dielectric layers, Annals of Physics 40 (1913) 817.
[34] C.G. Koops, On the dispersion of resistivity and dielectric constant of some semiconductors at audiofrequenies, Physical Review 83 (1951) 817.
[35] M. George, S.S. Nair, A.M. John, P.A. Joy, M.R. Anantharaman, Competing magnetic interactions in Nickel ferrite nanoparticle clusters; Role of magnetic interactions, Journal of Applied Physics 39 (2006) 900.
[36] I.H. Gull, A.Z. Abbasi, F. Amin, M.A. Rehman, A. Maqsood, Structural, magnetic and electrical properties of $Co_{1-x}Zn_xFe_2O_4$ synthesized by co-precipitation method, Journal of Magnetism and Magnetic Materials 311 (2007) 494.
[37] N. Rezlescue, E. Rezlescu, Study of strucrural and magnetic properties of Ni–Mg ferrites, Physica Status Solidi (a) 23 (1974) 575.
[38] M.A Gabal, Effect of Mg substitution on the magnetic properties of NiCuZn ferrite nanoparticles prepared through a novel method using egg white, Journal of Magnetism and Magnetic Materials 321 (2009) 3144–3148.
[39] A.M. Abo El Ata, F.M. Reicha, M.M. Ali, Transport and magnetic permeability study of $SrCu_{2-x/2}Ti_xFe_{16-x}O_{27}$ W-type hexaferrites, Journal of Magnetism and Magnetic Materials 292 (2005) 17–24.